Structure and Electronic Properties of Grain Boundaries in Earth-Abundant Photovoltaic Absorber $Cu_2ZnSnSe_4$

Junwen Li,[†] David B. Mitzi,[‡] and Vivek B. Shenoy[†,*]

[†]School of Engineering, Brown University, Providence, Rhode Island 02912, United States and, [‡]IBM T. J. Watson Research Center, Yorktown Heights, New York 10598, United States

ABSTRACT

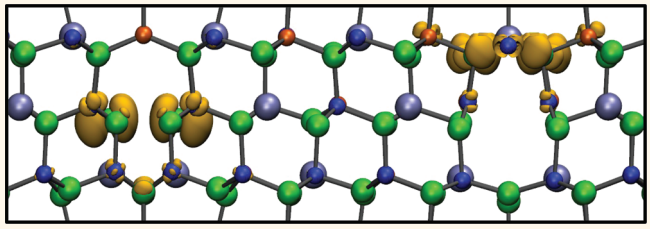

We have studied the atomic and electronic structure of $Cu_2ZnSnSe_4$ and $CuInSe_2$ grain boundaries using first-principles calculations. We find that the constituent atoms at the grain boundary in $Cu_2ZnSnSe_4$ create localized defect states that promote the recombination of photon-excited electron and hole carriers. In distinct contrast, significantly lower density of defect states is found at the grain boundaries in $CuInSe_2$, which is consistent with the experimental observation that $CuInSe_2$ solar cells exhibit high conversion efficiency without the need for deliberate passivation. Our investigations suggest that it is essential to effectively remove these defect states in order to improve the conversion efficiency of solar cells with $Cu_2ZnSnSe_4$ as photovoltaic absorber materials.

KEYWORDS: solar cells · grain boundaries · CZTS

Solar radiation is one of the cleanest energy sources of almost unlimited potential, delivering in an hour approximately the energy equivalent of the world's annual consumption[1] and, in a year, twice the combined capacity of all other renewable and nonrenewable reserves.[2] The main obstacle that has to be faced in order to make solar energy widely available is the development of low-cost, high-throughput, and reliable photovoltaic (PV) production methods. Thin-film solar cell materials are of particular interest because they can be fabricated in a cost-effective manner. The $CuIn_xGa_{1-x}Se_2$ (CIGS) thin-film cells have received considerable attention in the past decades, and the conversion efficiency has been improved up to 20.3%.[3] However, the fact that In and Ga are not earth-abundant does not allow for low-cost production of solar cells from these materials. Indium is expensive because of the large amount of consumption in solar cells and liquid crystal displays. $Cu_2ZnSnS_xSe_{4-x}$ (CZTS) is regarded as one of the alternatives for CIGS with In and Ga replaced by Zn and Sn, two earth-abundant elements. Great progress has been made in fabricating CZTS solar cells and improving their efficiency with various methods such as solution processing,[4] thermal evaporation,[5] sputtering,[6] and tuning the composition of nanocrystals.[7]

Since grain boundaries (GBs) are ubiquitous in the polycrystalline materials, extensive studies have been carried out to investigate their role in determining the efficiency of solar cells. In general, the grain boundaries are expected to create deep levels that act as recombination centers for the photon-excited electron and hole pairs.[8,9] This process is detrimental to charge separation required for the operation of solar cells. While grain boundaries are generally believed to be harmful to the performance of solar cells, high conversion efficiency can be obtained in CIGS solar cells without any need for deliberate passivation of the grain boundaries.[10] To understand the role of grain boundaries, different models have been proposed to study the electrically benign nature of the grain boundaries. Persson and Zunger[11] showed that Cu depletion at grain boundaries may create hole barriers through reduced coupling between Se p and Cu d orbitals. Yan *et al.*[12] found that the large relaxation of atomic structures at grain boundaries can pull the defect states into valence bands of bulk CIGS. Meanwhile, there are also a great deal of experimental investigations on the grain boundary of CIGS.[13−17] Despite the importance of grain boundaries in the thin-film solar cells and the potential for CZTS as a more cost-effective

* Address correspondence to vivek_shenoy@brown.edu.

Received for review June 9, 2011 and accepted October 18, 2011.

Published online October 18, 2011
10.1021/nn203230g

material compared to CIGS, there are very few studies on the structure and electronic properties of the grain boundaries in this material.[18] Most studies to date have focused on the physical properties of crystalline, defect-free materials.[19−24]

In the present article, we report first-principles calculations that examine the defect states of grain boundaries of kesterite $Cu_2ZnSnSe_4$ and chalcopyrite $CuInSe_2$ by using density functional theory. Our work shows the presence of defect states in the band gap of corresponding bulk crystal, derived from the Cu 3d and Se 4p orbitals at the grain boundaries in $Cu_2ZnSnSe_4$, underscoring the need for developing passivation schemes for improving conversion efficiency. The $CuInSe_2$ grain boundaries, in contrast, show significantly lower density of defect states which are mostly generated from Se 4p orbitals.

RESULTS AND DISCUSSION

The crystal structure of kesterite $Cu_2ZnSnSe_4$ can be derived from zinc blende *via* an intermediate chalcopyrite structure by using sequential cation cross-substitution.[25−27] In Figure 1, we depict the crystal structures of zinc blende CdTe, chalcopyrite $CuInSe_2$, and kesterite $Cu_2ZnSnSe_4$. In the zinc blende CdTe, the cation Cd and anion Te occupy two interpenetrating face-centered cubic (fcc) lattices independently. The chalcopyrite $CuInSe_2$ can be derived from the zinc blende structure by doubling the unit cell along the *c* axis and replacing Cd by ordered Cu and In on the cation fcc lattice and Te by Se. The kesterite $Cu_2ZnSnSe_4$ could be obtained by further substituting In with ordered Zn and Sn. In the process of structure derivation, anion atoms (Te, Se) are located at one fcc lattice while cations share the other one.

The atomic structures of grain boundaries in CIGS and CZTS materials remain unclear. However, we can model the grain boundaries of $CuInSe_2$ and $Cu_2ZnSnSe_4$ based on the experimental observations of the structures of grain boundaries in CdTe *via* high-resolution transmission electron microscopy (HRTEM)[9] because of the structural similarities between CdTe, $CuInSe_2$, and $Cu_2ZnSnSe_4$. Depending on the arrangement of constituent elements Cu, Zn, Sn, and Se, four different kinds of grain boundaries were constructed. Figure 2 and Figure 3 show the atomic structures of $Cu_2ZnSnSe_4$ grain boundaries. The grain boundary (114) plane is indicated by the dashed line. For convenience, the atomic sites at the grain boundary are numbered as 1, 2, ...6, as shown in Figure 2. A *n* is used to denote the atom A at position *n* and A*n*(−B*m*) denotes the atom A at position *n* bonded to atom B at position *m*. The four grain boundaries we consider can be distinguished by the combination of atom types at positions 1 and 6, as shown in Figure 2 for GB-I, II and Figure 3 for GB-III, IV. Both GB-I and GB-III have Se atoms at position 1.

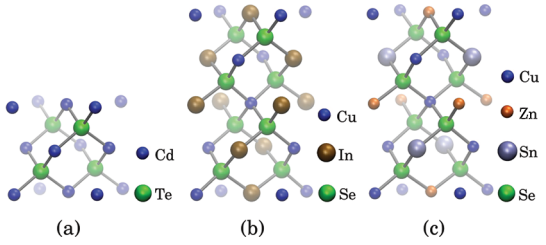

Figure 1. Schematic structures of (a) zinc blende CdTe, (b) chalcopyrite $CuInSe_2$, and (c) kesterite $Cu_2ZnSnSe_4$. The coloring scheme emphasizes the derivation of the kesterite structure from the zinc blende *via* the chalcopyrite structure.

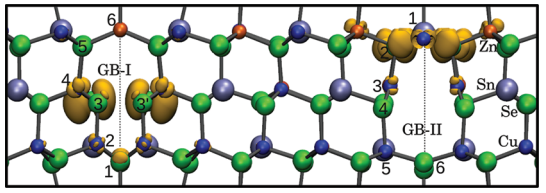

Figure 2. Relaxed atomic structure of $Cu_2ZnSnSe_4$ GBs. Left grain boundary is denoted as GB-I containing a Se core and alternating Cu and Zn at position 6. Right grain boundary is denoted as GB-II containing alternating Cu and Sn at position 1 and Se atom at position 6. The isosurfaces (yellow) set at 3×10^{-3} $e/Å^3$ represent the partial charge densities of energy states within the band gap of perfect $Cu_2ZnSnSe_4$.

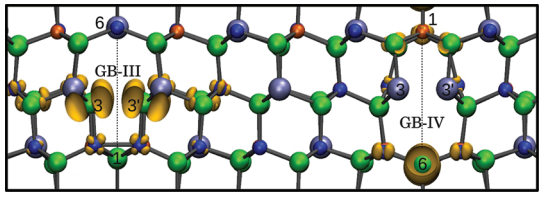

Figure 3. Relaxed atomic structure of $Cu_2ZnSnSe_4$ GBs. Left grain boundary is denoted as GB-III containing a Se core and alternating Cu and Sn at position 6. Right grain boundary is denoted as GB-IV containing alternating Cu and Zn at position 1 and Se at position 6. The isosurfaces (yellow) set at 3×10^{-3} $e/Å^3$ represent the partial charge densities of energy states within the band gap of perfect $Cu_2ZnSnSe_4$.

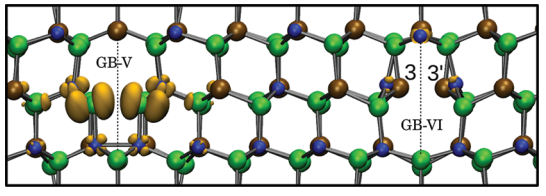

Figure 4. Relaxed atomic structure of $CuInSe_2$ GBs. Left grain boundary is denoted as GB-V containing a Se core. Right grain boundary is denoted as GB-VI containing a cation core. The isosurfaces (yellow) set at 3×10^{-3} $e/Å^3$ represent the partial charge densities of energy states within the band gap of perfect $CuInSe_2$.

At position 6, there are alternating Cu and Zn in GB-I, while in GB-III, Cu and Sn alternate. GB-II and GB-IV have Se atoms at position 6. At position 1, there are alternating Cu and Sn in GB-II, while in GB-IV, Cu and Zn alternate.

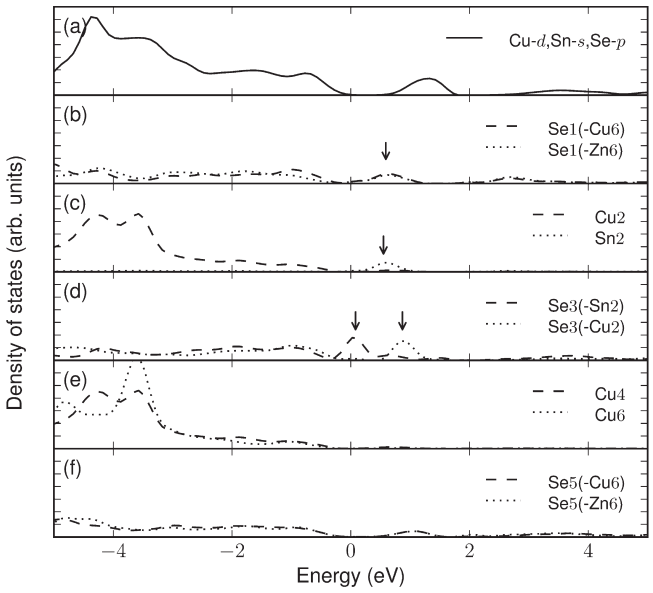

Figure 5. Projected density of states of $Cu_2ZnSnSe_4$ GB-I for (a) Cu, Sn, and Se at the bulk region of the supercell; (b) Se1 bonded to Cu6 and Zn6; (c) Cu and Sn at position 2; (d) Se3 bonded to Sn2 and Cu2; (e) Cu atoms at positions 4 and 6; (f) Se5 bonded to Cu and Zn at position 6. The 3d, 4s, and 4p orbitals are shown for Cu, Sn, and Se, respectively. The zero of the energy scale is set at the VBM of bulk $Cu_2ZnSnSe_4$, and the arrows indicate the peak positions of defect states. The corresponding partial charge densities ranging from VBM to CBM of perfect $Cu_2ZnSnSe_4$ are shown in Figure 2.

For $CuInSe_2$, two kinds of grain boundaries, GB-V with a Se core and GB-VI with a cation core, can be constructed and are presented in Figure 4. In addition to the atomic structures of GBs, in Figure 2, Figure 3, and Figure 4, we also depict the isosurfaces of partial charge densities to illustrate the localization of the defect states arising from grain boundaries.

First, we consider the structure of relaxed grain boundaries in $Cu_2ZnSnSe_4$. The grain boundary introduces bonds that are not tetrahedrally coordinated. Therefore, not all of the atoms at positions 1−6 as indicated in Figure 2 have coordination of four as the atoms in the bulk region of supercell. The atoms at position 1 are five-coordinated, the atoms at positions 2, 4, and 5 four-coordinated, and the remaining atoms at positions 3 and 6 are three-coordinated. After geometry optimization, the GB-I and GB-III show very little change in the structure while GB-II and GB-IV undergo dramatic structural relaxation. The Cu and Zn atoms at position 3 of GB-II that are bonded in the sp^3 configuration prior to relaxation become sp^2-bonded after relaxation. In GB-IV, only Cu3 atoms experience this bonding change from sp^3 to sp^2 while Sn3 atoms move toward the counterpart Sn3′ atoms to form dimers of distance 2.86 Å. The relaxed $CuInSe_2$ GB-V(VI) has atomic structures similar to that of $Cu_2ZnSnSe_4$ GB-III(IV). The GB-V shows little change in structure. In GB-VI, the In3 and In3′ form a dimer of distance 2.73 Å while Cu3 atoms undergo a transition from sp^3 to sp^2 configuration.

Second, because the changes in atomic structure can be expected to have an important effect on the electronic states around the Fermi level, we investigate the density of states projected onto the atoms at grain boundaries. For the crystalline $Cu_2ZnSnSe_4$, only Cu 3d, Se 4p, and Sn 4s orbitals play a role in determining the energy states near the Fermi level. The valence band maximum (VBM) is an antibonding state of Cu 3d and Se 4p orbitals, while the conduction band minimum (CBM) is an antibonding state of Sn 4s and Se 4p orbitals. Zn atoms do not contribute to the states near the Fermi level. In the analysis based on density of states (DOS) for grain boundaries, we only show the relevant orbitals such as Cu 3d, Sn 4s, and Se 4p. For $CuInSe_2$, the VBM is an antibonding state of Cu 3d and Se 4p orbitals while the CBM is an antibonding state of In 5s and Se 4p orbitals. Therefore, only Cu 3d, In 5s, and Se 4p orbitals are described. The projected density of states (PDOS) on these relevant orbitals for each grain boundary are presented in the following.

Figure 5 illustrates the PDOS of $Cu_2ZnSnSe_4$ GB-I. The peaks of defect states are indicated by arrows. As shown in Figure 5b,c, the defect states from Se1 and Sn2 are peaked at about 0.58 eV, which is close to the CBM. The Se3 atoms can bond to Cu and Sn atoms at position 2, and therefore, the Se3−Se3′ dimers may have two different bond lengths of 3.27 and 2.60 Å. The peaks in Figure 5d are derived from the antibonding interactions of 4p orbitals of the dimers. Since the interaction strength decreases with increasing bond length, the peaks at 0.08 and 0.87 eV are corresponding to the dimer lengths of 3.27 and 2.60 Å, respectively.

The PDOS of $Cu_2ZnSnSe_4$ GB-II are depicted in Figure 6. The defect states peaked at 0.26 eV in Figure 6b are from Cu atoms at position 1, while the defect states in Figure 6c are from Se atoms at position 2.

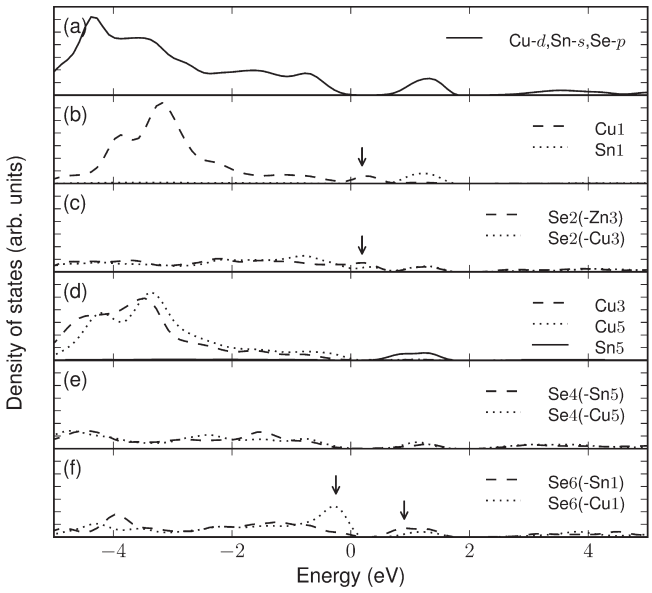

Figure 6. Projected density of states of $Cu_2ZnSnSe_4$ GB-II for (a) Cu, Sn, and Se at bulk region of supercell; (b) Cu and Sn at position 1; (c) Se2 bonded to Zn and Cu at position 3; (d) Cu at position 3 and Cu and Sn at position 5; (e) Se4 bonded to Cu and Sn at position 5; (f) Se6 bonded to Sn and Cu at position 1. The 3d, 4s, and 4p orbitals are shown for Cu, Sn, and Se, respectively. The zero of the energy scale is set at the VBM, and the arrows indicate the peak positions of defect states. The corresponding partial charge densities ranging from VBM to CBM of perfect $Cu_2ZnSnSe_4$ are shown in Figure 2.

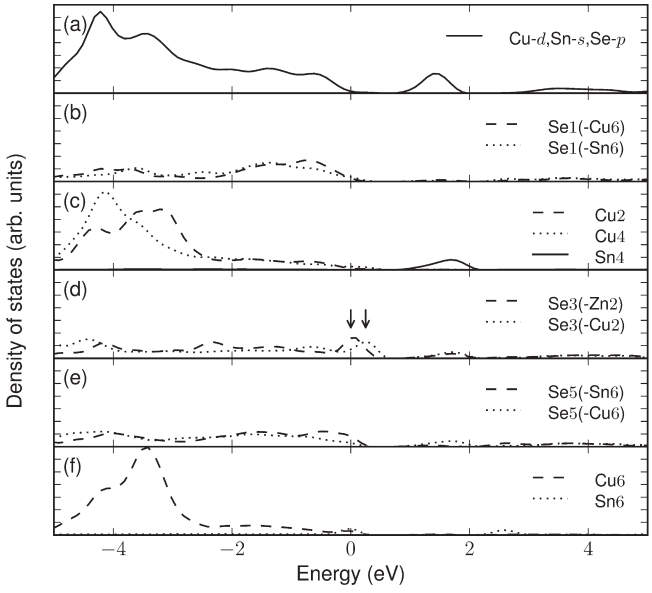

Figure 7. Projected density of states of $Cu_2ZnSnSe_4$ GB-III for (a) Cu, Sn, and Se at bulk region of supercell; (b) Se1 bonded to Cu and Sn at position 6; (c) Cu at position 2, Cu and Sn at position 4; (d) Se3 bonded to Zn and Cu at position 2; (e) Se5 bonded to Sn and Cu at position 6; (f) Cu and Sn at position 6. The 3d, 4s, and 4p orbitals are shown for Cu, Sn, and Se, respectively. The zero of the energy scale is set at the VBM, and the arrows indicate the peak positions of defect states. The corresponding partial charge densities ranging from VBM to CBM of perfect $Cu_2ZnSnSe_4$ are shown in Figure 3.

Although there are two peaks from Se6 atoms in Figure 6f, they are located in the valence and conduction bands.

In Figure 7, we present PDOS of $Cu_2ZnSnSe_4$ GB-III. The Se3−Se3′ dimers contribute to the antibonding states of 4p orbitals, which peak at 0.0 and 0.25 eV as in Figure 7d, corresponding to the dimer lengths of 3.15 and 2.85 Å, respectively.

Figure 8 describes the PDOS of $Cu_2ZnSnSe_4$ GB-IV. The defect states peaked at 0.1 eV in Figure 8b are due to Cu atoms at position 1. Defect states peaked at 0.1 and 0.2 eV from Se atoms at position 2 and 6 can be observed in Figure 8c,f, respectively.

To further illustrate the charge distribution of the defect states, we also calculated the partial charge densities which include the energy states ranging from

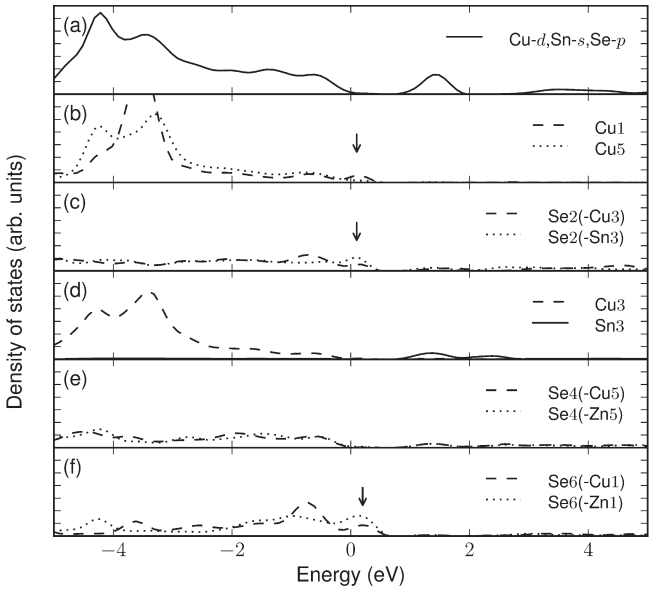

Figure 8. Projected density of states of $Cu_2ZnSnSe_4$ GB-IV for (a) Cu, Sn, and Se at bulk region of supercell; (b) Cu at position 1 and 5; (c) Se2 bonded to Cu and Sn at position 3; (d) Cu and Sn at position 3; (e) Se4 bonded to Cu and Zn at position 5; (f) Se6 bonded to Cu and Zn at position 1. The 3d, 4s, and 4p orbitals are shown for Cu, Sn, and Se, respectively. The zero of the energy scale is set at the VBM, and the arrows indicate the peak positions of defect states. The corresponding partial charge densities ranging from VBM to CBM of perfect $Cu_2ZnSnSe_4$ are shown in Figure 3.

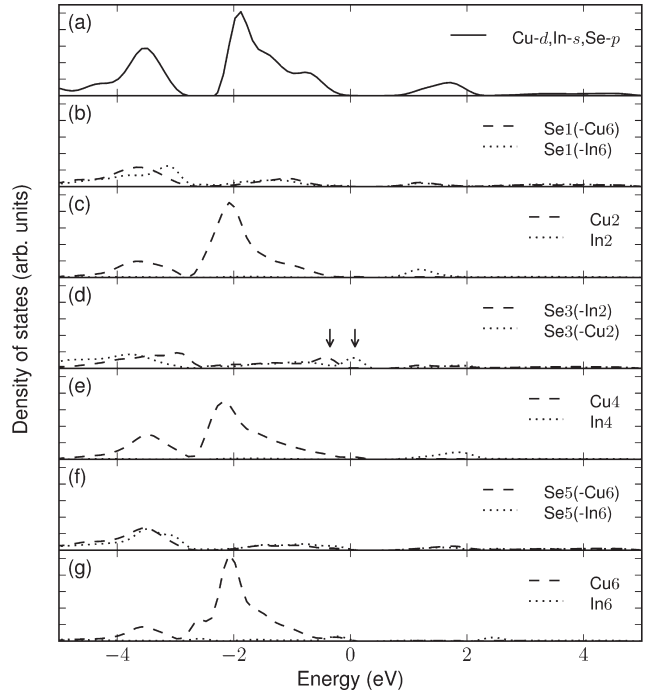

Figure 9. Projected density of states of $CuInSe_2$ GB-V for (a) Cu, Sn, and Se at bulk region of the supercell; (b) Se1 bonded to Cu and In at position 6; (c) Cu and In at position 2; (d) Se3 bonded to Cu and In at position 2; (e) Cu and In at position 4 and 6; (f) Se5 bonded to Cu and In at position 6; (g) Cu and In at position 6. The 3d, 5s, and 4p orbitals are shown for Cu, In, and Se, respectively. The zero of the energy scale is set at the VBM, and the arrows indicate the peak positions of defect states. The corresponding partial charge densities ranging from VBM to CBM of perfect $CuInSe_2$ are shown in Figure 4.

VBM to CBM of the bulk $Cu_2ZnSnSe_4$. We depict the isosurface plots of GB-I, II in Figure 2 and GB-III, VI in Figure 3, respectively. The isovalues are set at 3×10^{-3} $e/Å^3$. Note that the defect states are strongly localized near the dislocation core region. Only in GB-IV there is considerable contribution from Se6 atoms. This is consistent with our PDOS calculation results.

Compared to the grain boundaries in $Cu_2ZnSnSe_4$, the $CuInSe_2$ grain boundaries exhibit fewer defect states. We present the PDOS of $CuInSe_2$ GB-V in Figure 9.

Only the antibonding states caused by the Se3−Se3′ dimers bonded to Cu at position 2 are in the bulk gap. Although the Se3−Se3′ dimers bonded to In at position 2 create a peak, it is located at 0.35 eV below the VBM. In Figure 4, we plot the isosurface of partial charge density integrated from VBM to CBM for $CuInSe_2$ and set the isovalues at 3×10^{-3} e/Å^3. Figure 4a clearly suggests that the defect states in GB-V are mainly contributed by Se3 atoms. The GB-VI PDOS (not shown) exhibits no defect peaks in the bulk gap of $CuInSe_2$ as evidenced from the partial charge densities in Figure 4b. Yan *et al.*,[12] using the local density functional approximations (LDA), studied the $CuInSe_2$ grain boundaries and found that the defect states move into the bulk bands as a result of large structure relaxation. Our results on the $CuInSe_2$ obtained by using the EV-GGA density functional are qualitatively consistent with their work that adopts the LDA functional.

Because the CZTS is composed of earth-abundant elements and is environment friendly compared to CIGS, it is a promising candidate for low-cost thin-film solar cells. The current highest efficiency of 9.6% of CZTS cells[4] is still much lower than the record efficiency of around 20% of CIGS. Our results show that the deep levels at grain boundaries in CZTS facilitate the electron hole recombination and therefore are harmful to the conversion efficiency of the solar cell. In CIGS, the large relaxation experienced by atoms at the grain boundary plays a role of decreasing the defect states from the energy gap. The structure change, however, does not have a similar effect in CZTS compared to CIGS. The studies presented in the present work suggest that the grain boundary may be a factor limiting the efficiency of CZTS solar cell, and thus effective passivation treatment is needed to improve the efficiency.

CONCLUSIONS

In summary, we have carried out a study of the structure and electronic properties of grain boundaries in $Cu_2ZnSnSe_4$ and $CuInSe_2$ using density functional theory. We have found that the grain boundaries in $Cu_2ZnSnSe_4$ create more defect levels in the energy gap of bulk crystal compared to $CuInSe_2$. These defect states can promote the recombination of excited electron and hole carriers and should therefore be detrimental to the charge separation in the solar cell. Our work suggests that efficient passivation of these defect states should be necessary to improve the conversion efficiency of the solar cell with $Cu_2ZnSnSe_4$ as a photovoltaic absorber.

METHODS

The structures of $Cu_2ZnSnSe_4$ grain boundaries were optimized using the Vienna *ab initio* simulation package (VASP),[28] with exchange-correlation functional described by Perdew−Burke−Ernzerhof generalized gradient approximation (PBE-GGA)[29] and interaction between core electrons and valence electrons by the frozen-core projector-augmented wave (PAW) method.[30] An energy cutoff of 276 eV was used for plane wave basis expansion. The fully relaxed lattice constants a and c and tetragonal distortion parameter $\eta = c/2a$ that we obtain for crystalline $Cu_2ZnSnSe_4$ are a = 5.761 Å and η = 1.000, respectively. Our results are close to a = 5.763 Å and η = 0.998 obtained in previous computational work[19] as well as experimental studies (a = 5.68 Å and η = 1.00).[31] Although the widely used PBE-GGA density functional can well describe the total energies and geometries, it usually underestimates the energy gaps. For crystalline $Cu_2ZnSnSe_4$, PBE-GGA gives zero band gap while the experimental value is about 1.0 eV.[32] The energy gap of 0.85 eV can be obtained by using the correction of Heyd−Scuseria−Ernzerhof (HSE) functional.[33,34] The HSE hybrid functional calculation is computationally expensive and cannot be efficiently applied to large systems with defects, such as the grain boundaries here. Instead of HSE and PBE-GGA functionals, we use Engel and Vosko's generalized gradient approximation (EV-GGA) which is obtained by optimizing the exchange-correlation potential and can give better description of energy states.[35,36] The EV-GGA density functional in the form of Vanderbilt ultrasoft pseudopotentials[37] as implemented in Quantum-ESPRESSO[38] was used in the calculations of electronic properties. The self-interaction correction was also included by setting the on-site interaction Hubbard term to 5.0 eV for d orbitals of Cu, Zn, and Sn. An energy cutoff of 680 eV was adopted for the plane wave expansion of wave functions.

Similar to the calculations of grain boundaries in $Cu_2ZnSnSe_4$, we relaxed the structures of $CuInSe_2$ grain boundaries and calculated their electronic properties by using PBE-GGA and EV-GGA, respectively. An energy cutoff of 273 eV was employed for the relaxation and 680 eV for the electronic properties' calculations. The calculated lattice parameters are a = 5.870 Å and η = 1.007, which is in good agreement with the experimental results (a = 5.832 Å and η = 0.996).[39] During relaxation, all atoms in the supercells of $Cu_2ZnSnSe_4$ and $CuInSe_2$ were allowed to move until the force on each atom is less than 0.02 eV/Å.

Acknowledgment. We gratefully acknowledge research support of the NSF and NRI through the Brown University MRSEC program and the NSF through the Grants CMMI-0825771, DMS-0914648, and DMS-0854919.

REFERENCES AND NOTES

1. Morton, O. Solar Energy: A New Day Dawning? Silicon Valley Sunrise. *Nature* **2006**, *443*, 19–22.
2. Hermann, W. A. Quantifying Global Exergy Resources. *Energy* **2006**, *31*, 1685–1702.
3. Jackson, P.; Hariskos, D.; Lotter, E.; Paetel, S.; Wuerz, R.; Menner, R.; Wischmann, W.; Powalla, M. New World Record Efficiency for Cu(In,Ga)Se_2 Thin-Film Solar Cells Beyond 20%. *Prog. Photovoltaics* **2011**, DOI: 10.1002/pip.1078.
4. Todorov, T. K.; Reuter, K. B.; Mitzi, D. B. High-Efficiency Solar Cell with Earth-Abundant Liquid-Processed Absorber. *Adv. Mater.* **2010**, *22*, E156–E159.
5. Wang, K.; Gunawan, O.; Todorov, T.; Shin, B.; Chey, S. J.; Bojarczuk, N. A.; Mitzi, D.; Guha, S. Thermally Evaporated Cu_2ZnSnS_4 Solar Cells. *Appl. Phys. Lett.* **2010**, *97*, 143508.
6. Katagiri, H.; Jimbo, K.; Yamada, S.; Kamimura, T.; Maw, W. S.; Fukano, T.; Ito, T.; Motohiro, T. Enhanced Conversion Efficiencies of Cu_2ZnSnS_4-Based Thin Film Solar Cells by Using Preferential Etching Technique. *Appl. Phys. Express* **2008**, *1*, 041201.
7. Guo, Q.; Ford, G. M.; Yang, W.-C.; Walker, B. C.; Stach, E. A.; Hillhouse, H. W.; Agrawal, R. Fabrication of 7.2% Efficient CZTSSe Solar Cells Using CZTS Nanocrystals. *J. Am. Chem. Soc.* **2010**, *132*, 17384–17386.

8. Seto, J. Y. W. The Electrical Properties of Polycrystalline Silicon Films. *J. Appl. Phys.* **1975**, *46*, 5247–5254.
9. Yan, Y.; Al-Jassim, M. M.; Jones, K. M. Structure and Effects of Double-Positioning Twin Boundaries in CdTe. *J. Appl. Phys.* **2003**, *94*, 2976–2979.
10. Ramanathan, K.; Contreras, M. A.; Perkins, C. L.; Asher, S.; Hasoon, F. S.; Keane, J.; Young, D.; Romero, M.; Metzger, W.; Noufi, R.; Ward, J.; Duda, A. Properties of 19.2% Efficiency ZnO/CdS/CuInGaSe$_2$ Thin-Film Solar Cells. *Prog. Photovoltaics* **2003**, *11*, 225–230.
11. Persson, C.; Zunger, A. Anomalous Grain Boundary Physics in Polycrystalline CuInSe$_2$: The Existence of a Hole Barrier. *Phys. Rev. Lett.* **2003**, *91*, 266401.
12. Yan, Y.; Jiang, C.-S.; Noufi, R.; Wei, S.-H.; Moutinho, H. R.; Al-Jassim, M. M. Electrically Benign Behavior of Grain Boundaries in Polycrystalline CuInSe$_2$ Films. *Phys. Rev. Lett.* **2007**, *99*, 235504.
13. Siebentritt, S.; Sadewasser, S.; Wimmer, M.; Leendertz, C.; Eisenbarth, T.; Lux-Steiner, M. C. Evidence for a Neutral Grain-Boundary Barrier in Chalcopyrites. *Phys. Rev. Lett.* **2006**, *97*, 146601.
14. Yan, Y.; Noufi, R.; Al-Jassim, M. M. Grain-Boundary Physics in Polycrystalline CuInSe$_2$ Revisited: Experiment and Theory. *Phys. Rev. Lett.* **2006**, *96*, 205501.
15. Lei, C.; Li, C. M.; Rockett, A.; Robertson, I. M. Grain Boundary Compositions in Cu(InGa)Se$_2$. *J. Appl. Phys.* **2007**, *101*, 024909.
16. Mönig, H.; Smith, Y.; Caballero, R.; Kaufmann, C. A.; Lauermann, I.; Lux-Steiner, M. C.; Sadewasser, S. Direct Evidence for a Reduced Density of Deep Level Defects at Grain Boundaries of Cu(In,Ga)Se$_2$ Thin Films. *Phys. Rev. Lett.* **2010**, *105*, 116802.
17. Hafemeister, M.; Siebentritt, S.; Albert, J.; Lux-Steiner, M. C.; Sadewasser, S. Large Neutral Barrier at Grain Boundaries in Chalcopyrite Thin Films. *Phys. Rev. Lett.* **2010**, *104*, 196602.
18. Wang, K.; Shin, B.; Reuter, K. B.; Todorov, T.; Mitzi, D. B.; Guha, S. Structural and Elemental Characterization of High Efficiency Cu$_2$ZnSnS$_4$ Solar Cells. *Appl. Phys. Lett.* **2011**, *98*, 051912.
19. Chen, S.; Gong, X. G.; Walsh, A.; Wei, S.-H. Crystal and Electronic Band Structure of Cu$_2$ZnSnX$_4$ (X = S and Se) Photovoltaic Absorbers: First-Principles Insights. *Appl. Phys. Lett.* **2009**, *94*, 041903.
20. Ichimura, M.; Nakashima, Y. Analysis of Atomic and Electronic Structures of Cu$_2$ZnSnS$_4$ Based on First-Principle Calculation. *Jpn. J. Appl. Phys.* **2009**, *48*, 090202.
21. Paier, J.; Asahi, R.; Nagoya, A.; Kresse, G. Cu$_2$ZnSnS$_4$ as a Potential Photovoltaic Material: A Hybrid Hartree-Fock Density Functional Theory Study. *Phys. Rev. B* **2009**, *79*, 115126.
22. Persson, C. Electronic and Optical Properties of Cu$_2$ZnSnS$_4$ and Cu$_2$ZnSnSe$_4$. *J. Appl. Phys.* **2010**, *107*, 053710.
23. Mortazavi Amiri, N. B.; Postnikov, A. Electronic Structure and Lattice Dynamics in Kesterite-Type Cu$_2$ZnSnSe$_4$ from First-Principles Calculations. *Phys. Rev. B* **2010**, *82*, 205204.
24. Ichimura, M.; Nakashima, Y. Analysis of Atomic and Electronic Structures of Cu$_2$ZnSnS$_4$ Based on First-Principle Calculation. *Jpn. J. Appl. Phys.* **2009**, *48*, 090202.
25. Chen, S.; Gong, X. G.; Walsh, A.; Wei, S.-H. Electronic Structure and Stability of Quaternary Chalcogenide Semiconductors Derived from Cation Cross-Substitution of II-VI and I-III-VI$_2$ Compounds. *Phys. Rev. B* **2009**, *79*, 165211.
26. Goodman, C. H. L. The Prediction of Semiconducting Properties in Inorganic Compounds. *J. Phys. Chem. Solids* **1958**, *6*, 305–314.
27. Pamplin, B. A Systematic Method of Deriving New Semiconducting Compounds by Structural Analogy. *J. Phys. Chem. Solids* **1964**, *25*, 675–684.
28. Kresse, G.; Hafner, J. *Ab Initio* Molecular Dynamics for Liquid Metals. *Phys. Rev. B* **1993**, *47*, 558–561.
29. Perdew, J. P.; Burke, K.; Ernzerhof, M. Generalized Gradient Approximation Made Simple. *Phys. Rev. Lett.* **1996**, *77*, 3865–3868.
30. Blöchl, P. E. Projector Augmented-Wave Method. *Phys. Rev. B* **1994**, *50*, 17953–17979.
31. Babu, G. S.; Kumar, Y. B. K.; Bhaskar, P. U.; Raja, V. S. Effect of Post-deposition Annealing on the Growth of Cu$_2$ZnSnSe$_4$ Thin Films for a Solar Cell Absorber Layer. *Semicond. Sci. Technol.* **2008**, *23*, 085023.
32. Ahn, S.; Jung, S.; Gwak, J.; Cho, A.; Shin, K.; Yoon, K.; Park, D.; Cheong, H.; Yun, J. H. Determination of Band Gap Energy (E_g) of Cu$_2$ZnSnSe$_4$ Thin Films: On the Discrepancies of Reported Band Gap Values. *Appl. Phys. Lett.* **2010**, *97*, 021905.
33. Heyd, J.; Scuseria, G. E.; Ernzerhof, M. Hybrid Functionals Based On a Screened Coulomb Potential. *J. Chem. Phys.* **2003**, *118*, 8207–8215.
34. Heyd, J.; Scuseria, G. E.; Ernzerhof, M. Erratum: "Hybrid Functionals Based on a Screened Coulomb Potential". *J. Chem. Phys.* **2003**, *118*, 8207; *J. Chem. Phys.* **2006**, *124*, 219906.
35. Engel, E.; Vosko, S. H. Exact Exchange-Only Potentials and the Virial Relation as Microscopic Criteria for Generalized Gradient Approximations. *Phys. Rev. B* **1993**, *47*, 13164–13174.
36. Dufek, P.; Blaha, P.; Schwarz, K. Applications of Engel and Vosko's Generalized Gradient Approximation in Solids. *Phys. Rev. B* **1994**, *50*, 7279–7283.
37. Vanderbilt, D. Soft Self-Consistent Pseudopotentials in a Generalized Eigenvalue Formalism. *Phys. Rev. B* **1990**, *41*, 7892–7895.
38. Giannozzi, P.; Baroni, S.; Bonini, N.; Calandra, M.; Car, R.; Cavazzoni, C.; Ceresoli, D.; Chiarotti, G. L.; Cococcioni, M.; Dabo, I.; *et al.* QUANTUM ESPRESSO: A Modular and Open-Source Software Project for Quantum Simulations of Materials. *J. Phys.: Condens. Matter* **2009**, *21*, 395502.
39. Jaffe, J. E.; Zunger, A. Theory of the Band-Gap Anomaly in ABC$_2$ Chalcopyrite Semiconductors. *Phys. Rev. B* **1984**, *29*, 1882–1906.